Dynamic strength, particle deformation, and fracture within fluids with impact-activated microstructures

Oren E. Petel, and Simon Ouellet

Citation: Journal of Applied Physics **122**, 025108 (2017); doi: 10.1063/1.4990982
View online: http://dx.doi.org/10.1063/1.4990982
View Table of Contents: http://aip.scitation.org/toc/jap/122/2
Published by the American Institute of Physics

Dynamic strength, particle deformation, and fracture within fluids with impact-activated microstructures

Oren E. Petel[1,a)] and Simon Ouellet[2]
[1]*Department of Mechanical and Aerospace Engineering, Carleton University, Ottawa, Ontario K1S 5B6, Canada*
[2]*Defence Research and Development Canada Valcartier, Québec, Québec G3J 1X5, Canada*

(Received 16 February 2017; accepted 17 June 2017; published online 12 July 2017)

The evolution of material strength within several dense particle suspensions impacted by a projectile is investigated and shown to be strongly dependent on the particle material in suspension. For stronger particles, such as silicon carbide, the shear strength of the fluid is shown to increase with the ballistic impact strength. For weaker particles, such as silica, the shear strength of the suspension is found to be independent of impact strength in this dynamic range of tests. A soft-capture technique is employed to collect ejecta samples of a silica-based shear thickening fluid, following a ballistic impact and penetration event. Ejecta samples that were collected from impacts at three different velocities are observed and compared to the benchmark particles using a Scanning Electron Microscope. The images show evidence of fractured and deformed silica particles recovered among the nominally 1 μm diameter monodisperse spheres. There is also evidence of particle fragments that appear to be the result of interparticle grinding. The trends observed in the shear strength estimates are interpreted with regards to the particle damage seen in the ejecta recovery experiments to develop a concept of the impact response of these fluids. The results suggest that particle slip through deformation is likely the dominant factor in limiting the transient impact strength of these fluids. Particularly, particle strength is important in the formation and collapse of dynamically jammed particle contact networks in the penetration process.
[http://dx.doi.org/10.1063/1.4990982]

I. INTRODUCTION

Armor applications of shear thickening fluids (STFs) have received considerable attention[1–10] due to their field-responsive nature,[11,12] although ballistic performance limitations against steel projectiles remain a concern.[1,4,13–15] Early investigations on the ballistic performance of silica-based STFs demonstrated that they were ineffective against steel-core or copper-jacketed lead rounds, despite their ability to deform and stop lead projectiles.[1,2] In recent years, similar silica-based STFs have been used as an interstitial component embedded in ballistic fabrics or composite panels to create stimulus-responsive protective equipment for ballistic,[3–6,16–19] stab,[7,20–22] shock wave,[23] and hypervelocity threats.[8–10] Ballistic results with STF-fabric armor systems have demonstrated poor performance against steel projectiles at velocities above 300 m/s.[4,13] The source of this performance limitation remains unclear, although recent work on ballistic penetration of STFs suggests that it is caused by a strength limitation of the particle sub-phase.[14,15,24] Under transient high-strain-rate loading, the response of STFs is strongly influenced by the material properties of the suspended solid particle sub-phase,[25,26] influencing the penetration response of the STFs.[14,15,27] A study of STF impact face ejecta suggested a model of progressive particle damage at increasing impact velocities that was linked to observed variations in ejecta kinetic energy distributions and a diminishing role of interparticle friction at the impact face.[24]

STFs typically consist of a dense particle sub-phase suspended in a Newtonian fluid medium that exhibits a shear strain-rate-dependent increase in viscosity, due to microstructure effects from its suspended particles.[11,12] Competing approaches to capture the dynamic response of STFs have involved elastohydrodynamic models that couple lubrication forces to the elastic deformation of the particles through Hertzian contact mechanics[28,29] and models that include direct frictional contact definitions between particles.[30–32] Under impact loading at intermediate strain rates, direct interparticle interactions have been shown to influence the response of STFs,[33–35] with recent efforts focusing on direct visualization of the transiently shear-jammed regions of particles.[36–38] At higher strain rates, the strength of the particle sub-phase was directly related to the dynamic stress transfer within dense suspensions.[25,26,39]

Investigations into the effect of particle hardness on STF-fabric systems measured higher ballistic limits among single-layer fabrics when silica, as opposed to the softer polymethylmethacrylate particles, was embedded in the fabric.[27] A similar link between particle strength and ballistic performance was found in penetration studies of fluid targets containing cornstarch, silica, and silicon carbide particles.[14,15] In testing above 300 m/s, the ballistic resistance of the silica-based STF appears to converge to an inertial response with minimal evidence of material strength effects.[14,15,40] It was suggested that the role of the particle sub-phase in the STFs is diminished significantly at increasing impact velocities, possibly due to deformation of the particles under the high stress load of the impacts.[14,15,24] A

a)oren.petel@carleton.ca

computational investigation of ballistic impacts of steel projectiles on an STF-impregnated fabrics suggests peak impact stresses on the order of 1 GPa.[41] Given the role of particle contacts in transient shear jamming within STFs[36–38] and the magnitude of stress fluctuations seen at contact points within granular media,[42] the local stresses of particle contact sites could exceed 1 GPa under ballistic loading. It is therefore not surprising that particle deformation or even damage may be an important factor in limiting the ballistic response of an STF.

While grain crushing has been reported in packed-beds of dry granular systems for ballistic impact velocities exceeding 100 m/s,[43,44] the prospect of grain crushing has not received significant attention in liquid-saturated particle systems. During the penetration process of a granular bed, grains are displaced to allow the projectile to penetrate the medium. This process of rearrangement involves granular rotation and translation; however, grain crushing becomes increasingly important at higher strain rates.[45] The limited data available on the penetration of liquid-saturated particle beds have demonstrated that the fluid reduces the resistance of the granular material to penetration.[46,47] This change in the dynamic response of the packed bed granular systems may be due to soil liquefaction or the fluid behaving as a lubricant between frictional grain contacts during rearrangement.[45] Both of these mechanisms would reduce the propensity for grain crushing during penetration within a saturated particle system and may reduce its effective strength in resisting penetration. These two mechanisms may not be as relevant at elevated strain rates, increasing the likelihood of particle deformation as a dominant penetration mechanism.

The prospect of STF particle damage limiting the strength of the suspension during impact deserves further analysis. In this study, a penetration model is used to estimate the resistive shear strength of several STFs during projectile penetration. The evolution of these resistive stresses with impact velocity provides a basis of discussion with regards to particle deformation within STFs under extreme loading conditions. An experimental ballistic ejecta recovery technique is used to investigate deformation among particles recovered from the impacted fluids. The combined results from the model and recovery experiments are presented in the context of previous high-strain-rate experiments and ballistic results.

II. PENETRATION MODEL

The ballistic penetration of suspensions has previously been successfully modelled as an area-modified plugging process.[15] These experiments measured the impact and residual velocities of a fragment simulating projectile (FSP) penetrating suspensions with variations in particle materials and volume fractions (see Fig. 1). The experimental deviations from an inertial (hydrodynamic) response were measured for several of the suspensions considered;[15] however, that analysis did not determine the resistive shear strength of the suspensions or its variation during penetration, information which would provide a more complete description of the penetration process. The penetration model is extended to estimate the average resistive shear stress acting to

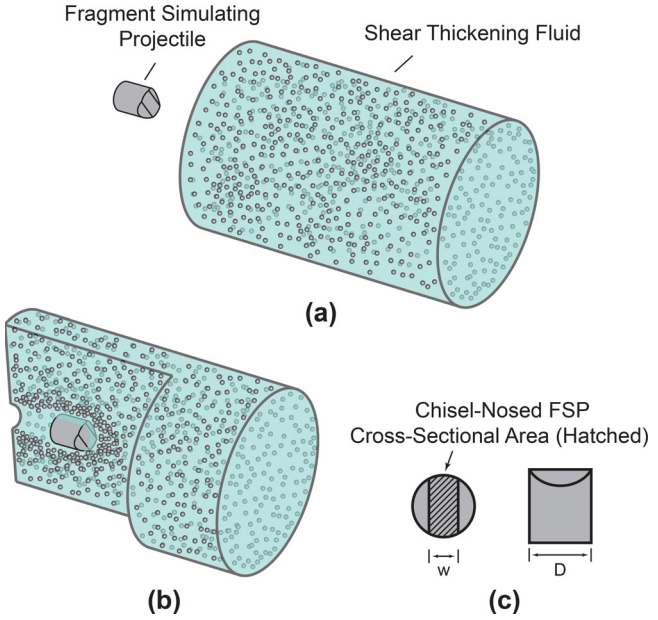

FIG. 1. Schematic of an STF suspension (a) in equilibrium prior to impact and (b) a broken-out section view of the projectile penetrating the suspension. (c) Top and side views of a chisel-nosed FSP. Taken from Ref. 15.

decelerate the projectile. Mixture details of the suspensions pertinent to this analysis are given in Table I and their rheological characterizations are shown in Fig. 2.

The model development starts with a statement of energy conservation describing the complete penetration of the target,[48] assuming that the projectile drives a plug within the target

$$\frac{1}{2}M_{\mathrm{fsp}}V_i^2 = \frac{1}{2}M_{\mathrm{fsp}}V_r^2 + \frac{1}{2}M_pV_r^2 + E_{\mathrm{fn}} + W, \tag{1}$$

where M_p is the mass of the plug formed from the target material, M_{fsp} is the mass of the projectile, E_{fn} is the energy of the projectile lost to the inertial response of a perfectly plastic impact, W is the work involved in the penetration process, and V_i and V_r are the incident and residual velocities of the projectile, respectively. The perfectly plastic energy loss term, which can also be seen as the inertial energy loss to the fluid assuming no material strength (E_{fn}), results from conserving momentum for an impact involving a perfectly plastic plug formation[48]

$$E_{\mathrm{fn}} = \frac{M_p}{M_{\mathrm{fsp}} + M_p} \cdot \frac{1}{2}M_{\mathrm{fsp}}V_i^2. \tag{2}$$

TABLE I. Summary of suspension properties.[15] All suspensions used ethylene glycol as a suspending medium.

Mixture	Particle material	Volume fraction (%)	ρ (kg/m^3)	$\beta_{50\,\mathrm{mm}}$	$\beta_{64\,\mathrm{mm}}$
21 SiC	Silicon carbide	21.5	1560	0.95	1.18
41 SiC	Silicon carbide	41.0	1977	1.20	1.50
48 SiC	Silicon carbide	48.0	2120	1.29	1.61
54 CS	Cornstarch	54.0	1349	0.82	1.02
61 SiO_2	Silica	61.5	1560	0.95	1.18
61 mix	Silica and silicon carbide	61.5	1757	1.07	1.33

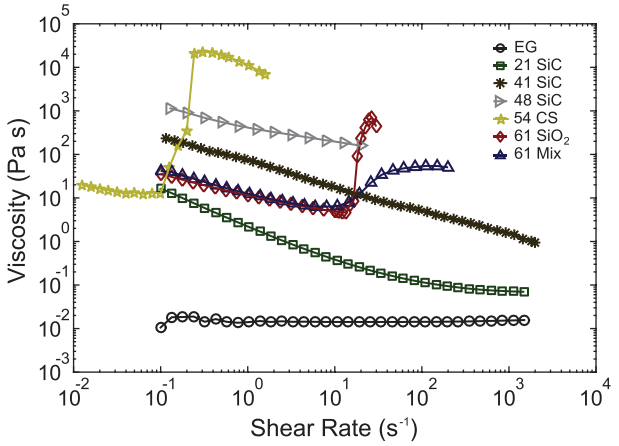

FIG. 2. A rheological characterization of the various mixtures described in Table I. Taken from Ref. 15.

The projectile used in the experiments was a chisel-nosed FSP, as seen in Fig. 1. A shape correction factor (A_r) is included in the plug mass term to account for the fact that the flat portion of the FSP nose is driving the plug. Hence, the plastic work term can be expressed as

$$W = \frac{M_{fsp}}{2}\left[\left(\frac{1}{1+\beta}\right)V_i^2 - (1+\beta)V_r^2\right], \tag{3}$$

$$\beta = \frac{\rho_p L_p A_r}{\rho_{fsp} L_{fsp}}, \tag{4}$$

where β is the ratio of plug to projectile mass and approximated by the expression, A_r is the cross-sectional area ratio between the plug formed and the projected area of the FSP, L is the axial length, ρ is the density, and the subscripts "*fsp*" and "*p*" refer to the projectile and plug, respectively.

At the limit of A_r equal to unity, the plug will have the same diameter as the FSP, while the value of A_r for the chisel-nosed FSP is given by the expression

$$A_r = 1 - \frac{1}{\pi}\cdot(\theta - \sin\theta), \tag{5}$$

$$\theta = 2\cos^{-1}\left(\frac{w}{D}\right), \tag{6}$$

where w is the width and D is the major diameter defining the flat nose region on the FSP, nominally 2.54 mm and 5.46 mm, respectively. Including this area ratio in the analysis of this dataset provides an accurate scaling of the residual velocity data.[15]

Examining the plastic work term for the plug, a reasonable estimate of the average resistive shear strength of the suspensions can be calculated using the expression

$$\tau_{av} = \frac{M_{fsp}}{2P_{fsp}L_p^2}\left[\left(\frac{1}{1+\beta}\right)V_i^2 - (1+\beta)V_r^2\right], \tag{7}$$

where τ_{av} is the average resistive shear stress and P_{fsp} is the perimeter of the flat-nosed portion of the FSP, which is given by

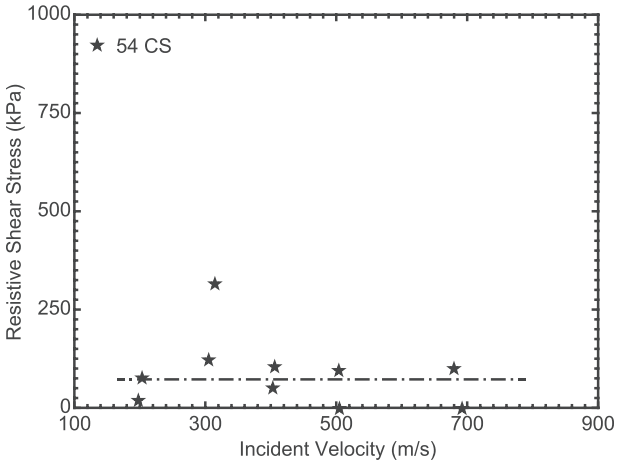

FIG. 3. The average resistive shear stress as a function of impact velocity for suspensions containing cornstarch.

$$P_{fsp} = 2D\cdot\sin^{-1}\left(\frac{w}{D}\right) + 2\sqrt{D^2 - w^2}. \tag{8}$$

Using the expression derived in Eq. (7) and published residual velocity data,[15] the average shear stress resisting the penetration of the FSP can be compared for several mixtures over a range of impact velocities. These results are presented in Figs. 3–5, where suspensions containing cornstarch, silica, and silicon carbide are plotted together in Figs. 3, 4, and 5, respectively. The results for 61 mix are presented in both Figs. 4 and 5, as this suspension contains both silicon carbide and silica. Linear trendlines have been added to the data for visualization purposes. Negative resistive shear stress values are non-physical within the model, as such, negative values are represented by a resistive stress of zero.

Two main trends are evident in the resistive shear stress data presented in Figs. 3–5, a constant shear stress independent of impact strength and a shear strength that increases with impact strength. These two trends highlight the differences in the impact responses of the particle sub-phases of these suspensions. The result of plate impact experiments on similar dense suspensions would suggest that the preferential

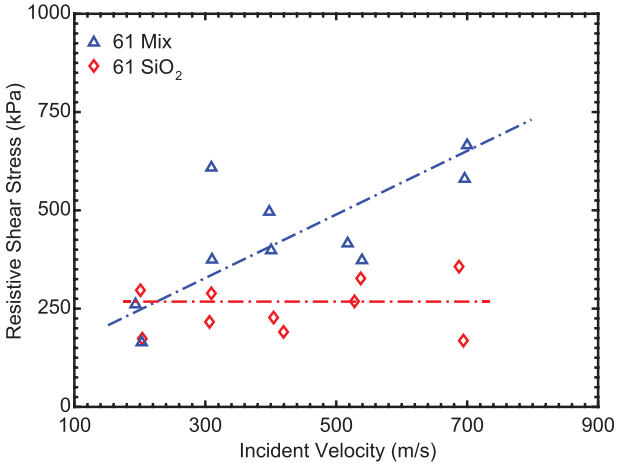

FIG. 4. The average resistive shear stress as a function of impact velocity for suspensions containing silica.

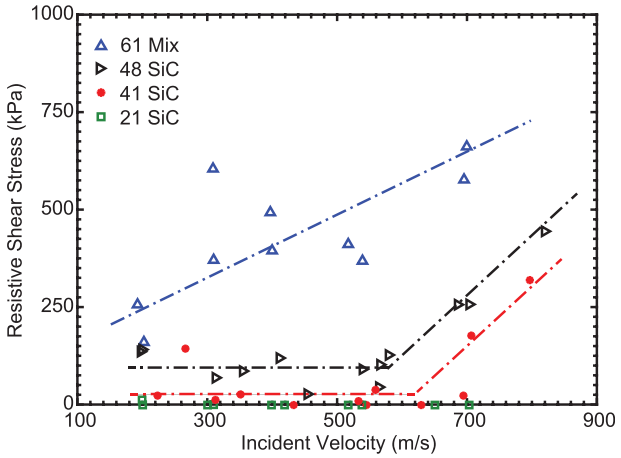

FIG. 5. The average resistive shear stress as a function of impact velocity for suspensions containing silicon carbide.

compression of the fluid medium should result in an increasing particle volume fraction at increasing impact strengths.[25,49] Therefore, one would expect the strength of every suspension tested to increase with loading strength; however, this is not seen for every mixture. In fact, an increase in shear strength is only seen for mixtures containing silicon carbide and only if they have sufficiently high volume fractions. For instance, the shear thickening cornstarch mixture shows a nearly constant and non-zero value of resistive shear stress (Fig. 3). A similar trend is seen for the suspension with silica particles (61 SiO_2), albeit with a higher average shear stress (Fig. 4). In contrast, the suspension 61 mix exhibits a shear strength that increases under increasing impact strengths (Fig. 4). This mixture is essentially based on 61 SiO_2, although a portion of silica particles are replaced with silicon carbide particles while maintaining the same particle volume fraction of 61.5%.

The results for the silicon carbide suspensions (Fig. 5) show elements of both trends. In the dilute silicon carbide mixture (21 SiC), there is no evidence of a measurable shear strength, as was to be expected. Increasing the volume fraction of the suspension to 41% or 48% results in non-zero resistive shear stresses that are independent of impact strength in the lower velocity range; however, the trend changes above 600 m/s.

At these higher impact speeds, both mixtures appear to exhibit a marked increase in resistive shear strength that may be indicative of a microstructural effect within the suspensions. The response of the silicon carbide mixtures is similar to the compression-induced stiffening seen in these same mixtures in plate impact testing over the identical velocity ranges.[25] The onset of an increasing strength in the silicon carbide mixtures of 41% and 48% volume fraction appears to be indicative of a transient shear jamming-type response,[36] where the increased stress load of the higher velocity impact brings the particles into closer contact, although in this case it was driven in part by compression of the fluid phase.[25,49] At low impact speeds, the compaction of the fluid is not sufficient to result in a jammed particle sub-phase,[49] resulting in a constant shear strength within the mixtures.

TABLE II. Summary of the bulk-material properties for the solid particle materials.

Material	ρ (kg/m^3)	E (GPa)	Hardness (GPa)	Refs.
Cornstarch	1550	4.9	Not available	51
Silica (amorph.)	2200	69.3	8.3	52
Silicon carbide	3220	454.7	30.8	52

This bi-linear trend in the shear strength relationship is not seen in the cornstarch and silica suspensions, despite their considerably higher volume fractions. Based on plate impact experiments with dense suspensions,[25] one would expect that the particles in these mixtures would be driven into their jammed regime, given their initial volume fractions. For instance, at a volume fraction of 61.5%, such as in the 61 SiO_2 suspension, the mixture should reach its jamming limit at all of the impact strengths investigated; however, this is not apparent from the trends in Fig. 4. The only suspensions that exhibit an increasing shear strength are those incorporating silicon carbide, the stiffest of the three particle materials (see material properties in Table II). The contrasting trends between the two suspensions in Fig. 4 with identical particle volume fractions, but different compositions, demonstrates that an increasing resistive shear strength with impact conditions is linked to the strength of the particles.

For the ballistic penetration of monolithic metallic plates, the resistive shear stress is a weak function of impact strength, since the materials are undergoing plastic flow.[50] The trends in Figs. 3 and 4, where the shear strength is constant for both cornstarch and silica suspensions, may be indicative of significant particle deformation, similarly resulting in a resistive shear strength independent of impact strength. This possibility needs to be confirmed experimentally, as the prospect of substantial particle deformation under ballistic loading has significant implications for the design of ballistic protection involving STFs.

III. EXPERIMENTAL DETAILS

An experimental investigation was undertaken to recover and examine ejecta particles from the backface of an impacted silica-based particle suspension sample (61 SiO_2). This suspension contained monodisperse silica spheres with a nominal diameter of 1 μm (obtained from Fiber Optic Center) dispersed in ethylene glycol at a volume fraction of 61.5%. A polyvinylchloride capsule with an internal diameter of 8 mm and a thickness of 6 mm was used to confine samples, as seen in Fig. 6. The polymer capsule was chosen in order to reduce the possible influence of lateral confinement on the response of the particles. Mylar diaphragms with a thickness of 0.1 mm were used to confine the fluid axially. A 17-grain NATO-standard chisel-nosed FSP was chosen for consistency with the data modelled in Sec. II. Backface ejecta was recovered from samples impacted at three velocities (258 m/s, 496 m/s, and 673 m/s).

A schematic of the experiment is given in Fig. 6. The path of the projectile leads from the sample to a 25-mm-thick

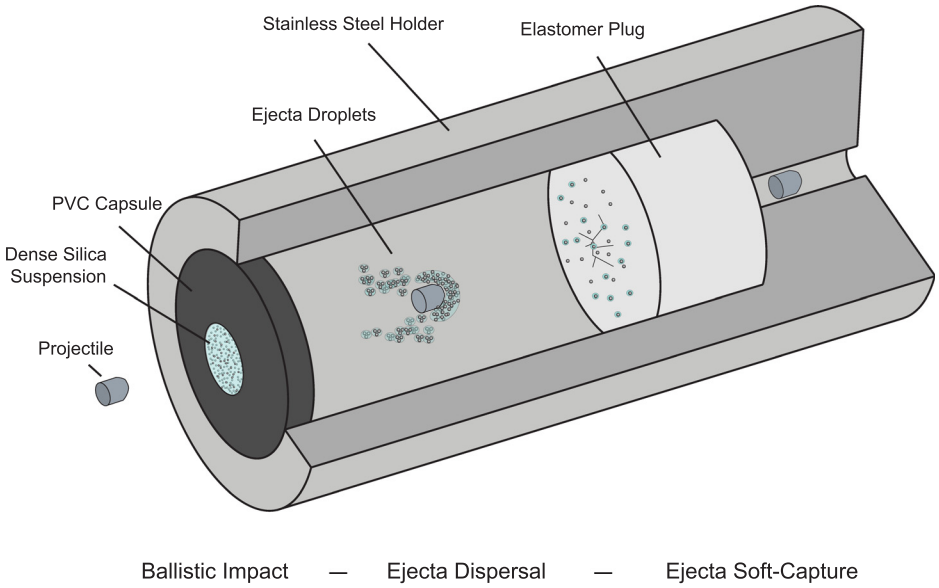

FIG. 6. A schematic of the experimental configuration sequentially prior to impact, during the projectile exit and ejecta dispersal phase, and soft-capture phase.

Sylgard 184 elastomer plug, which provided a soft-capture medium for the ejecta. The elastomer plug was used to strip particles from the passing FSP without damaging the particles further. Our analysis was limited to those particles that were trapped within the internal fractures of the elastomer, following the penetration of the projectile. The PVC capsule was supported within a cylindrical stainless steel holder at a distance of 150 mm from the front surface of the elastomer plug. Immediately behind the elastomer plug, a hole was drilled with sufficient clearance to allow the projectile to exit the holder.

Following each experiment, the elastomer plug was recovered and processed to ensure that only those particles trapped within the elastomer itself were investigated. The recovery process involved several steps: (i) the first 5 mm of the impact face of the plug was cut and removed; (ii) a similar 5 mm thick portion on the backface of the plug was removed to eliminate any contamination from the holder; (iii) the central core of the elastomer plug including the complete perforation and fracture zone was extracted; and (iv) the extracted portion of the plug was placed in a petri dish, sectioned into three parts and rinsed thoroughly with ethanol to recover the particles. The resulting solution of ethanol, ethylene glycol, and recovered particles was moved to a larger (25 ml) container and diluted further with additional ethanol. The sealed container was placed in an ultrasonic bath for 5 min and a sample of the solution was withdrawn by pipette. The withdrawn samples were deposited on several aluminum stands, allowing the ethanol to evaporate prior to imaging. All micrographs were taken using a Hitachi SU8010 series scanning electron microscope.

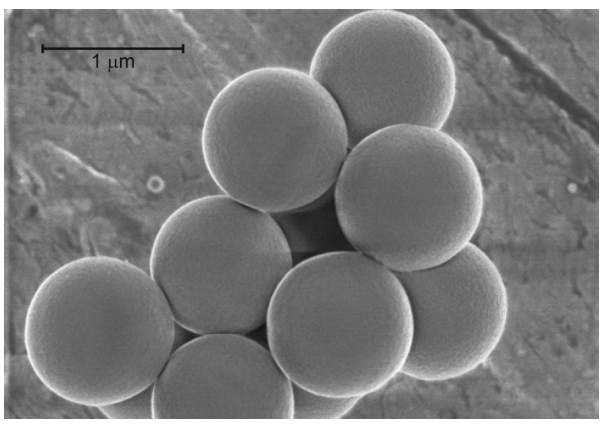

FIG. 7. SEM micrograph of the benchmark silica particles.

The benchmark samples of the particles were similarly withdrawn from the initial suspension (without being subjected to an impact) and subsequently processed for imaging using ethanol as described previously. A scanning electron microscope image of the benchmark particles is shown in Fig. 7. The average particle size measured in the benchmark suspension was $1.045 \pm 0.050\ \mu$m with a spherical morphology. There was no evidence of deformed or fragmented particles within the benchmark samples.

IV. RESULTS

A series of SEM micrographs are presented of the silica particles that were recovered from the impact experiments. Although many images were taken, these images represent the most severe damage seen among the particles imaged. Among these images, there appears to be a progression of damage evidence that correlates with impact velocity. At the lowest impact velocity investigated, 258 m/s, the recovered particles did not show evidence of fractured or permanently deformed particles. At the intermediate impact velocity of 496 m/s, the images contained evidence of silica particle fragments (Fig. 8). The irregular morphology of these fragments as well as the appearance of their fracture surfaces suggest that they resulted from interparticle frictional grinding from tangential contact between particles.

At the highest impact velocity investigated, 673 m/s, the damage to the recovered silica particles was far more dramatic (Fig. 9). These images show evidence of fractured particles as well as particle fragments. In the center of Fig. 9(a), a particle appears to have been significantly deformed under a compressive load. A similar observation is made in Fig. 9(b), where a

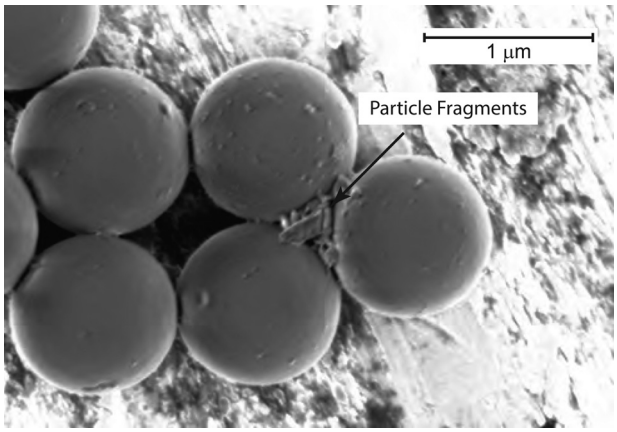

FIG. 8. Micrograph of recovered particles from an impact at 496 m/s.

particle at the center of the micrograph appears to have fractured under shear. Significant concentrations of particle fragments suspended within the interstitial regions between particles are also present in these images.

The number of particles observed with the level of deformation seen in Fig. 9 was quite limited, several out of the thousands of particles observed. There are a couple of immediate explanations for the low number of deformed particles observed. The projectile drives a significant plug of material ahead of it, the majority of the particles in this plug and recovered in the elastomer were not located along the plug periphery, where the highest shear stresses are present. Another aspect to consider is that deformation of a jammed structure requires particles to slip past one another; however, this does not necessitate large scale deformation of the particles to enable slip, as suggested by the recovered particle fragments in Figs. 8 and 9. Evidence of silica particle fragments were collected at the two higher impact velocities, indicating significant inelastic deformation of the particles under these impact conditions.

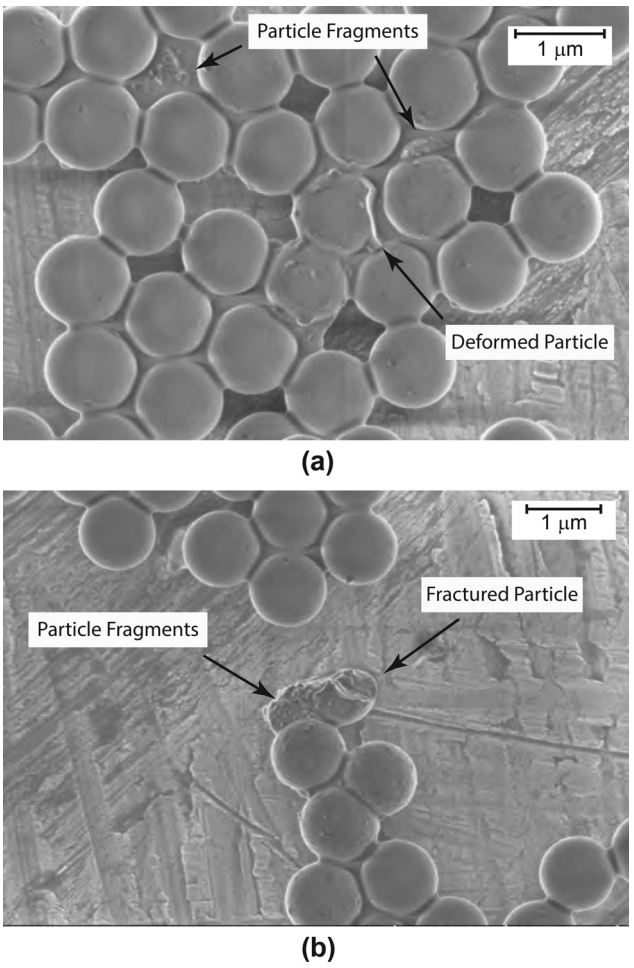

FIG. 9. Micrographs of recovered particles from an impact at 673 m/s.

V. DISCUSSION

Ballistic penetration of an STF is driven by the continual formation and destruction of force chains between contacting particles that resist the penetration. While STFs are typically used as an interstitial within ballistic fabrics, integrated particles are subjected to stress levels that are equivalent to this direct impact scenario on the fluid itself. Therefore, if particle fracture is a concern in an STF impact configuration, it should be considered as a potential concern in any ballistic or high-strain-rate application. The analysis of ballistic data with the penetration model illustrates that there are significant loads being carried between the particles in an STF during a ballistic impact event. While the average resistive shear stresses involved in the penetration process are seemingly quite low, this is due to averaging the stresses at contact sites over the full perimetral area of the plug. When concentrated over the area at the particle contact sites, these stresses can be quite significant. This is evident from the particle recovery experiments, where fragments of silica particles as well as particles exhibiting large deformations were recovered. A progression of damage with increasing impact velocities, from ground fragments to significantly deformed particles, should be expected as the imposed strain rate increases, reducing the available timescales for lateral particle mobility and reorganization during compaction. The finer fragments observed among the recovered ejecta particles provide evidence of fracture surfaces that were the result of tangential slip at frictional contact sites within the jammed structure, leading to fine-scale fragmentation.

In a dilute suspension, 21 SiC, particles do not come into contact to form jammed structures as the volume fraction is quite low. At elevated volume fractions, the particles must slip past one another to allow the passage of the FSP. These particle interactions may be elastic in nature involving rotation and translation of the particles or result in permanent particle deformation. In either scenario, the jammed particle structures are formed and destroyed to allow the penetration of the FSP. At increasing impact velocities, the proportion and extent of inelastic interactions between particles can be expected to increase. As the mean stress of the impact increases, the yield strength of a particle provides an upper limit on the stress necessary to destroy the jammed structures within the STF. The recovery experiments indicate that this limit is between 258 m/s and 496 m/s for silica particles impacted by a steel projectile, which is consistent with ballistic tests on STFs.[4,13] Any significant level of deformation

would limit the ability of the particles to maintain their resistance to penetration, rearranging the transiently jammed microstructure of particles to the detriment of their penetration resistance.

This yield limit is evident from the analysis of the penetration model, where STFs containing weaker particles (54 CS and 61 SiO_2) exhibit a shear strength independent of impact strength (Figs. 3 and 4). This suggests that the silica- and cornstarch-based suspensions are being limited by the material strength of the particles themselves. There is a statistical distribution of stresses within the contact sites of jammed structure,[42] resulting in particle deformations within the jammed particle microstructure. While most contact sites may be elastic between contacting particles, the largest contact stresses at elevated impact velocities results in a proportion of particles grinding past each other or even significantly deforming, as shown by the ejecta recovery results. A comparison of the 61 mix and 61 SiO_2 suspensions demonstrates that the addition of silicon carbide particles into the silica suspension at an identical volume fraction appeared to have stabilized the microstructure under dynamic loading. This is evident from the increasing resistive shear strength of 61 mix as a function of impact strength (Fig. 4). The presence of the stronger silicon carbide particle dominates the response of the mixture at high strain rates, buffering the deformation of the silica to increase its resistance to penetration.

The 61 mix and 61 SiO_2 suspensions allow a comparison of two material systems with identical volume fractions and similar rheological responses, where the only variation is the material properties and morphology of the particles. Based on the previous ballistic results pertaining to STF-fabric systems containing particles with varying morphology, from spherical to elongated ellipsoidal, the spherical particles were shown to absorb more energy at elevated volume fractions.[53] Based on those previous observations, particle morphology was not be considered to have had a dominant contribution to the result of the present study, since the mixture containing irregular silicon carbide particles outperformed the mixture with spherical silica particles.

In suspensions containing silicon carbide particles at lower volume fractions (41% and 48%), the shear strengths of the suspensions show both trends of behavior (Fig. 5). For these mixtures, the silicon carbide particles maintain mobility at low impact strengths, allowing reorganization of the microstructure with limited interparticle contact sites. As the impact strength is increased, the relative compressibility of the ethylene glycol medium leads to an effective increase in the particle volume fraction, as seen in plate impact testing.[25] The compression of the fluid brings the particle microstructure into a dynamically jammed state. It is expected that this compaction-induced transiently jammed system should be more stable with increasing impacting strength, resulting in increased coordination among particles due to the increased local volume fraction.[49] The expectation for increased coordination among particles is an increase to the resistive shear stress (as seen in 41 SiC, 48 SiC, and 61 mix results in Fig. 5), unless the material strength of the particles does not allow for it. For instance, the expected trend is not seen among the cornstarch (Fig. 3) and silica (Fig. 4) particle suspensions, due to particle deformation or fracture. In contrast, the silicon carbide particles are less susceptible to deformation and thus the microstructural reorganization that leads away from the jammed structures, resulting in the observed trend of increasing shear strength (Fig. 5). The critical impact strength at which this occurs in the 41 SiC and 48 SiC mixtures is identical to the impact strength for which it was measured in previous plate impact experiments, a material velocity above 500 m/s.[25] All of the suspensions containing silicon carbide undergo a strengthening due increasing impact strength conditions, so as long as they have a sufficient initial volume fraction to form a jammed structure. This result demonstrates that the compression-induced stiffening of the suspensions, a mechanism proposed in previous work,[25,49] may be of more relevance at these stress states and strain rates than classical rheological behaviour, particularly given the impact conditions of the present study.

The leading mechanism for the destruction of the particle chain microstructures within an STF is localized deformation or frictional particle grinding, enabling particle slip. Although particle fracture is occurring among silica and cornstarch particles at the higher impact velocities, the expectation of added energy absorption required to fracture these particles does not appear to have significantly factored into the amount of plastic work done by the FSP, the dynamic strength of those STFs, or the ballistic resistance of the suspensions. In other words, if the destruction of particle contact networks is necessary as the projectile penetrates, whether the microstructure is reorganized through particle frictional surface grinding and deformation or a combination of these mechanisms coupled with occasional particle fracture, there is no appreciable difference in the resistive shear strength of the STF. In ballistic experiments on STF fluids, Gates reasoned that the instantaneous hardness of the fluid must surpassed that of the projectile, finding that this was the case for lead bullets, but not for steel or copper, explaining the disparity in the performance against various munitions.[1,2] The results of this study concerning the deformation of silica particles under impact provides further support of this statement, given that the strength of the particles themselves were exceeded by steel projectiles at relevant impact velocities. These results similarly provide an explanation for the bounds on the ballistic performance of STF-integrated ballistic fabrics that has been seen experimentally.[4,13]

VI. CONCLUSIONS

Using an extended penetration model for STFs, we were able to determine the evolution of the resistive shear strength of various particle suspensions to penetration. The trends of the data provided insight into the particle-level response within these fluids during impact, particularly the role of particle material strength and deformation on the impact-resisting microstructure within a dynamically jammed suspension. For silicon carbide particle suspensions, the shear strength of the fluid is shown to increase with the impact strength. For weaker particles, such as silica, the shear strength of the suspension is independent of the impact

strength in the range of ballistic impacts studied, suggesting that particle slip through deformation and fracture is likely the dominant factor in limiting the transient impact strength of these fluids and that a yield limit is reached within the bounds of interest for ballistic protections.

The backface ejecta from a ballistic impact into a silica-based STF was successfully collected using a soft-capture technique to further investigate the possibility of particle deformation. Evidence of particle fragments was found in the collected ejecta at the two higher impact velocities examined, although completely fractured or significantly deformed particles were only seen within the ejecta collected at the highest impact velocity. The smaller particle fragments are due to interparticle grinding, although further investigation is merited. The observation of particle fracture within an STF during a ballistic impact event illustrates the importance of particle deformation under high-strain-rate loading. We have used these results to describe a conceptual interpretation of the dynamic behavior of STFs under ballistic impact. Our particular focus was the importance of particle strength and the role of the formation and collapse of dynamically jammed particle contact networks in the penetration process.

ACKNOWLEDGMENTS

The authors thank Jacques Blais for his assistance in conducting the experiments and microscopy. O. E. Petel acknowledges the financial support of the Natural Sciences and Engineering Research Council of Canada discovery grant program.

[1]L. E. Gates, Jr., Air Force Materials Laboratory Report No. AFML-TR-68-362 (1968).
[2]L. E. Gates, Jr., U.S. patent 3,649,426 (14 March 1972).
[3]Y. S. Lee, E. D. Wetzel, and N. J. Wagner, J. Mater. Sci. **38**, 2825 (2003).
[4]V. B. C. Tan, T. E. Tay, and W. K. Teo, Int. J. Solids Struct. **42**, 1561 (2005).
[5]J. L. Park, B. I. Yoon, J. G. Paik, and T. J. Kang, Text. Res. J. **82**, 527 (2012).
[6]M. Fahool and A. R. Sabet, Int. J. Impact Eng. **90**, 61 (2016).
[7]M. J. Decker, C. J. Halbach, C. H. Nam, N. J. Wagner, and E. D. Wetzel, Compos. Sci. Technol. **67**, 565 (2007).
[8]A. Bohannan and E. Fahrenthold, Int. J. Impact Eng. **35**, 1497 (2008).
[9]C. D. Cwalina, R. D. Dombrowski, C. J. McCutcheon, E. L. Christiansen, and N. J. Wagner, Procedia Eng. **103**, 97 (2015).
[10]J. Warren, K. R. Kota, S. M. Westberg, T. Lacy, S. Kundu, H. Toghiani, and C. U. Pittman, Jr., in *American Society of Composites, 30th Technical Conference* (Destech Publications, 2015).
[11]R. L. Hoffman, Trans. Soc. Rheol. **16**, 155 (1972).
[12]J. F. Brady and G. Bossis, J. Fluid Mech. **155**, 105 (1985).
[13]J. L. Park, B. I. Yoon, J. G. Paik, and T. J. Kang, Text. Res. J. **82**, 542 (2012).
[14]O. E. Petel, S. Ouellet, J. Loiseau, B. J. Marr, D. L. Frost, and A. J. Higgins, Appl. Phys. Lett. **102**, 064103 (2013).
[15]O. E. Petel, S. Ouellet, J. Loiseau, D. L. Frost, and A. J. Higgins, Int. J. Impact Eng. **85**, 83 (2015).
[16]Y. Park, Y. Kim, A. Baluch, and C. Kim, Compos. Struct. **125**, 520 (2015).
[17]E. Haro, A. Odeshi, and J. Szpunar, Int. J. Impact Eng. **96**, 11 (2016).
[18]Z. Tan, L. Zuo, W. Li, L. Liu, and P. Zhai, Mater. Des. **94**, 105 (2016).
[19]A. Majumdar, B. Butola, and A. Srivastava, Mater. Des. **54**, 295 (2014).
[20]T. Hassan, V. Rangari, and S. Jeelani, Mater. Sci. Eng., A **527**, 2892 (2010).
[21]X. Gong, Y. Xu, W. Zhu, S. Xuan, W. Jiang, and W. Jiang, J. Compos. Mater. **48**, 641 (2014).
[22]M. Hasanzadeh, V. Mottaghitalab, H. Babaei, and M. Rezaei, Composites A **88**, 263 (2016).
[23]A. Haris, H. P. Lee, T. E. Tay, and V. B. C. Tan, Int. J. Impact Eng. **80**, 143 (2015).
[24]O. E. Petel and J. D. Hogan, Int. J. Impact Eng. **93**, 39 (2016).
[25]O. E. Petel and A. J. Higgins, J. Appl. Phys. **108**, 114918 (2010).
[26]A. S. Lim, S. L. Lopatnikov, N. J. Wagner, and J. W. Gillespie, Jr., Rheol. Acta **49**, 879 (2010).
[27]D. P. Kalman, R. L. Merrill, N. J. Wagner, and E. D. Wetzel, Appl. Mater. Interfaces **1**, 2602 (2009).
[28]S. P. Meeker, R. T. Bonnecaze, and M. Cloitre, Phys. Rev. Lett. **92**, 198302 (2004).
[29]J. Mewis and N. J. Wagner, *Colloidal Suspension Rheology* (Cambridge University Press, 2012).
[30]E. Brown and H. M. Jaeger, J. Rheol. **56**, 875 (2012).
[31]N. Fernandez, R. Mani, D. Rinaldi, D. Kadau, M. Mosquet, H. Lombois-Burger, J. Cayer-Barrioz, H. J. Herrmann, N. D. Spencer, and L. Isa, Phys. Rev. Lett. **111**, 108301 (2013).
[32]R. Seto, R. Mari, J. F. Morris, and M. M. Denn, Phys. Rev. Lett. **111**, 218301 (2013).
[33]S. R. Waitukaitis and H. M. Jaeger, Nature **487**, 205 (2012).
[34]S. R. Waitukaitis, L. K. Roth, V. Vitelli, and H. M. Jaeger, Europhys. Lett. **102**, 44001 (2013).
[35]M. Roché, E. Myftiu, M. C. Johnston, P. Kim, and H. A. Stone, Phys. Rev. Lett. **110**, 148304 (2013).
[36]E. Han, I. R. Peters, and H. M. Jaeger, Nat. Commun. **7**, 12243 (2016).
[37]I. R. Peters and H. M. Jaeger, Soft Matter **10**, 6564 (2014).
[38]R. Maharjan, S. Mukhopadhyay, B. Sokol, B. Allen, T. Storz, and E. Brown, e-print arXiv:1407.0719v3.
[39]O. E. Petel, D. L. Frost, A. J. Higgins, and S. Ouellet, AIP Conf. Proc. **1426**, 1495 (2012).
[40]O. E. Petel, AIP Conf. Proc. **1793**, 120022 (2017).
[41]B. Lee and C. Kim, Adv. Compos. Mater. **21**, 177 (2012).
[42]D. W. Howell, R. P. Behringer, and C. T. Veje, Chaos **9**, 559 (1999).
[43]W. A. Allen, E. B. Mayfield, and H. L. Morrison, J. Appl. Phys. **28**, 370 (1957).
[44]S. J. Bless, D. T. Berry, B. Pedersen, and W. Lawhorn, AIP Conf. Proc. **1195**, 1361 (2009).
[45]M. Omidvar, M. Iskander, and S. J. Bless, Int. J. Impact Eng. **66**, 60 (2014).
[46]L. E. Malvern, R. L. Sierakowski, C. A. Ross, J. E. Milton, and C. S. Ting, Air Force Amament Laboratory Report No. AFATL-TR-76-129 (1976).
[47]J. O. Marston, I. U. Vakarelski, and S. T. Thoroddsen, Phys. Rev. E **86**, 020301 (2012).
[48]R. F. Recht and T. W. Ipson, J. Appl. Mech. **30**, 384 (1963).
[49]O. E. Petel, D. L. Frost, A. J. Higgins, and S. Ouellet, Phys. Rev. E **85**, 021401 (2012).
[50]Z. Rosenberg and E. Dekel, Int. J. Solids Struct. **46**, 4169 (2009).
[51]S. R. Waitukaitis, "Impact-activated solidification of cornstarch and water suspensions," Ph.D. thesis (The University of Chicago, 2013), p. 136.
[52]G. M. Pharr, Mater. Sci. Eng. A **253**, 151 (1998).
[53]E. Wetzel, Y. Lee, R. Egres, K. Kirkwood, J. Kirkwood, and N. Wagner, AIP Conf. Proc. **712**, 288 (2014).